Controlled-NOT logic with nonresonant Josephson phase qubits

Andrei Galiautdinov*
Department of Physics and Astronomy, University of Georgia, Athens, Georgia 30602, USA
(Received 23 December 2008; published 13 April 2009)

We establish theoretical bounds on qubit detuning for some of the previously proposed controlled-NOT (CNOT) logic gate implementations with *weakly* coupled Josephson phase qubits. It is found that in the two-step, $\sqrt{i\mathrm{SWAP}}$-based case the value of the detuning during the entangling operations must not exceed $2g$, where g is the characteristic coupling constant. In the single-step case we consider two practical, physically distinct implementations, in which one of the qubits is driven by a concurrent rf pulse of fixed frequency. We find that when the local drive is applied to the "reference" qubit (with which it is in resonance), the detuning should not exceed g. If the drive is applied to the "detuned" qubit, generation of the perfect CNOT gate is possible at any value of detuning provided that the amplitude of the pulse can be made arbitrarily large.

DOI: 10.1103/PhysRevA.79.042316 PACS number(s): 03.67.Lx, 03.65.Fd, 85.25.−j

I. INTRODUCTION

The majority of the entangling gate designs proposed for solid-state quantum computing architectures assume that during the entangling pulses the qubits are maintained on strict resonance [1–8] (see Refs. [9,10] for notable exceptions). This is hardly surprising since in the rotating wave approximation (RWA) typically used to analyze *weakly* coupled superconducting qubits such resonant condition leads to relatively simple and easily solvable Hamiltonians containing no local σ_k^z terms. This prescription works well when the system consists of only two qubits. However, if thousands of such qubits are assembled into an integrated circuit, maintaining them on resonance may become a difficult task. In that case, architecture's ability to reliably generate universal gates at finite detuning would be of great practical importance.

Such detuning flexibility may also become an asset if it is found that for some applications the use of qubits with intrinsically different level splittings is advantageous or outright necessary. Another issue that may arise when designing a quantum computer is the possibility of making uncontrollable errors during the fabrication process, which would prevent the qubits from being tuned to resonance exactly. It would be useful to have an architecture that is sufficiently robust and capable of executing perfect entangling operations in the presence of such defects.

At present, in actual experiments, detuning is routinely used to "decouple" the qubits in order to perform local (that is, nonentangling) operations [1,11–13]. It would be convenient if, after such decoupling is performed, the qubits did not have to be brought back to resonance when doing subsequent, *entangling* operations. Also, from the purely theoretical standpoint, decoupling provides a useful limit against which to check our calculations. If at larger detuning the interaction is expected to lose its entangling properties, we have to be able to predict a crossover into the regime when the gate fidelity [of the controlled-NOT (CNOT), in our case] begins to deteriorate. Thus, the primary goal of this paper will be to investigate the possibility of generating controlled-NOT logic gates at finite detuning and to establish the exact conditions under which the crossover occurs in some of the previously proposed implementations.

To develop a good intuition when analyzing the crossover, we will make extensive use of the following analytical tools.

To compare the Makhlin invariants $G_{1,2}(\xi,t)$ [14] of various entangling gates $U(\xi,t)$ with those of controlled-NOT,

$$G_1(\mathrm{CNOT})=0, \quad G_2(\mathrm{CNOT})=1, \tag{1}$$

we define the distance from the CNOT class by

$$d(\xi,t) := \sqrt{|G_1(\xi,t)|^2+[G_2(\xi,t)-1]^2}, \tag{2}$$

where ξ stands for various available controls (such as, for example, Rabi frequencies and detuning) and t is the time to do the entangling operation. Here we used the fact that quite generally, $G_1\in\mathbb{C}$, $G_2\in\mathbb{R}$ [cf. Eq. (6)]. The distance function introduced in Eq. (2) is *not* a measure of the gate fidelity. Infinitely many gates, all differing from each other by arbitrary local rotations, may have the same value of d. Once the entangling part of the gate is found to have $d=0$, it can then be made into the canonical CNOT gate by additional local rotations,

$$U(\xi,t)\rightarrow e^{i\phi}R_{\mathrm{post}}U(\xi,t)R_{\mathrm{pre}}=\mathrm{CNOT}\equiv\begin{pmatrix}1&0&0&0\\0&1&0&0\\0&0&0&1\\0&0&1&0\end{pmatrix}, \tag{3}$$

where an extra phase ϕ accounts for $\det(\mathrm{CNOT})=-1$.

Actual experiments motivate this choice of the distance function. It is generally believed that doing local rotations is easy, but performing entanglement is difficult. Thus, if by using experimentally available interaction and the local controls we can somehow steer the system into the "right" equivalence class, then making the actual target gate would be relatively straightforward.

Mathematically, the utility of the distance function comes from the fact that exact CNOTs correspond precisely to its singular points, as can be seen by taking the gradient,

*ag@physast.uga.edu

$$\partial_{\xi,t} d = \frac{\mathrm{Re}(G_1)\partial_{\xi,t}\,\mathrm{Re}(G_1) + \mathrm{Im}(G_1)\partial_{\xi,t}\,\mathrm{Im}(G_1) + (G_2-1)\partial_{\xi,t} G_2}{\sqrt{|G_1|^2 + (G_2-1)^2}}. \tag{4}$$

In situations when analytical solution cannot be found, such singularities can be easily identified on the graph of $d(\xi,t)$. The approximate values of local controls needed to generate a CNOT gate can then be read off the graph and used as a seed for a search, such as, for instance, Nelder-Mead simplex direct search with bound constraints.

To visualize how various elements of the CNOT class are actually reached in the course of the unitary evolution we simulate the Weyl chamber steering trajectories $\vec{c}(t) = (c_1(t), c_2(t), c_3(t))$ for the appropriate values of control parameters. The goal here is to establish a correspondence [15],

$$U(\xi,t) \leftrightarrow U_{\vec{c}(\xi,t)} = e^{-(\pi/2)[c_1(\xi,t)XX + c_2(\xi,t)YY + c_3(\xi,t)ZZ]}, \tag{5}$$

between the physical gate $U(\xi,t)$ and the unphysical matrix exponential $U_{\vec{c}(\xi,t)}$ that formally resides in the same local equivalence class as $U(\xi,t)$. The time-dependent vector $\vec{c}(t)$ then represents the dynamically generated local class at every moment of system's evolution. In general, the class vectors and the Makhlin invariants are related by

$$\begin{aligned} G_1 &= \cos^2(\pi c_1/2)\cos^2(\pi c_2/2)\cos^2(\pi c_3/2) \\ &\quad - \sin^2(\pi c_1/2)\sin^2(\pi c_2/2)\sin^2(\pi c_3/2) \\ &\quad + (i/4)\sin(\pi c_1)\sin(\pi c_2)\sin(\pi c_3), \\ G_2 &= 4\cos^2(\pi c_1/2)\cos^2(\pi c_2/2)\cos^2(\pi c_3/2) \\ &\quad - 4\sin^2(\pi c_1/2)\sin^2(\pi c_2/2)\sin^2(\pi c_3/2) \\ &\quad - \cos(\pi c_1)\cos(\pi c_2)\cos(\pi c_3). \end{aligned} \tag{6}$$

For the CNOT class, the standard choice is

$$\vec{c}(\mathrm{CNOT}) = (1,0,0). \tag{7}$$

Other class vectors representing the CNOT class can be made from this one by any combination of (a) shifts by 2 units along any of the c axes, e.g., $(c_1,c_2,c_3) \to (c_1+2,c_2,c_3)$, (b) reverses of any two components, e.g., $(c_1,c_2,c_3) \to (-c_1,-c_2,c_3)$, and (c) swaps of any two components, e.g., $(c_1,c_2,c_3) \to (c_2,c_1,c_3)$.

Finally, we define the intrinsic fidelity of the entangling gate with respect to the target CNOT by

$$\begin{aligned} \mathcal{F} &:= 1 - \mathrm{tr}\{[U_{\vec{c}} - U_{(1,0,0)}]^\dagger [U_{\vec{c}} - U_{(1,0,0)}]\} \\ &= -7 + 2\cos[(\pi/4)(c_1 + c_2 + c_3 - 1)] \\ &\quad + 2\cos[(\pi/4)(c_1 - c_2 + c_3 - 1)] \\ &\quad + 2\cos[(\pi/4)(c_1 + c_2 - c_3 - 1)] \\ &\quad + 2\cos[(\pi/4)(c_1 - c_2 - c_3 - 1)], \end{aligned} \tag{8}$$

where the second equality was established by direct calculation.

Our general strategy for generating controlled-NOT logic at finite detuning will thus involve two major steps: (a) finding the optimized entangling gate $U_{\mathrm{opt}} \equiv U(\xi_{\mathrm{opt}}, t_{\mathrm{opt}})$ that minimizes the distance function $d(\xi,t)$ and (b) finding the corresponding class vector $\vec{c}_{\mathrm{opt}}$ that gives the intrinsic fidelity of U_{opt}.

Since there is an infinite number of possible local drives and rotating frames to choose from, it will be necessary to limit our discussion to situations that are simple and yet powerful enough to provide some interesting physical insights. Our specific choices for Rabi pulses and rotating frames will be made in Eqs. (11), (12), (14), (35), (36), (41), (42), (52), and (53).

The paper is organized as follows.

In Sec. III we generalize to finite detuning the familiar two-step CNOT sequence involving a local π pulse sandwiched between two $\sqrt{i\mathrm{SWAP}}$ entangling operations. The exact bound on detuning that guarantees generation of the perfect (in the RWA) controlled-NOT logic gate will then be given in Eq. (26).

In Sec. IV generalization to finite detuning is performed with the help of two physically different single-step CNOT implementations. In Sec. IV B 1 we consider the case in which, during the entangling operation, a concurrent rf drive resonant with the reference qubit is applied. We will see that in that case the restriction on detuning for perfect CNOT generation is somewhat stronger than in the two-step case [Eq. (46)].

In Sec. IV B 2 we apply the same rf drive to the "detuned" qubit and find that in this case perfect CNOT generation is possible at any value of detuning provided that the amplitude of the pulse can be chosen to be sufficiently large. We conclude in Sec. V with a brief summary of our results.

II. NOTATION

In what follows, we will use the notation that is convenient for Lie algebraic manipulations:

$$\begin{aligned} X_k &= \frac{i}{2}\sigma_k^x, \quad Y_k = \frac{i}{2}\sigma_k^y, \quad Z_k = \frac{i}{2}\sigma_k^z, \quad (k=1,2), \\ XX &= \frac{i}{2}\sigma_2^x\sigma_1^x, \quad YY = \frac{i}{2}\sigma_2^y\sigma_1^y, \quad ZZ = \frac{i}{2}\sigma_2^z\sigma_1^z, \\ XY &= \frac{i}{2}\sigma_2^x\sigma_1^y, \quad YX = \frac{i}{2}\sigma_2^y\sigma_1^x. \end{aligned} \tag{9}$$

Notice that $[XX,YY]=[XY,YX]=0$, and ZZ commutes with each of the XX, YY, XY, and YX operators.

Why is this notation convenient? Consider the following transformation (called "going to a rotated frame") on the Lie algebra su(4) of the two-qubit system:

$$XX \to e^{-\theta Z_1} XX e^{\theta Z_1} = XX\cos\theta + XY\sin\theta. \tag{10}$$

This transformation can be nicely interpreted as a rotation of vector XX by an angle θ in the *real* vector space spanned by the generators of the group SU(4). This is how the continuous group acts on its Lie algebra. Mathematicians call it the adjoint representation. The algebra plays the role of the representation space for its own group. Since we do work at the level of algebra, and not at the level of the Hilbert space when discussing equivalence classes of gates, this is a very convenient notation. It simplifies things. Also notice how naturally the periodicity of 2π appears at this level of description.

Now, if we were to write the same transformation in terms of the Pauli matrices, we would have to remember to put in the imaginary unit i and the factors of 1/2 in the exponents on the left-hand side of Eq. (10),

$$e^{-i\theta\sigma_z^1/2}(\sigma_2^x\sigma_1^x)e^{i\theta\sigma_z^1/2} = (\sigma_2^x\sigma_1^x)\cos\theta + (\sigma_2^x\sigma_1^y)\sin\theta,$$

breaking its beautiful symmetry.

III. TWO-STEP CNOT

A. Hamiltonian

When restricted to the computational subspace, the Hamiltonian for two coupled Josephson phase qubits (no rf drives yet) is given by

$$iH(t) = -\epsilon(Z_1+Z_2) - \delta Z_2 + 2(g_{xx}XX + g_{yy}YY + (\tilde{g}/2)ZZ + \ldots), \tag{11}$$

where $g_{xx}, g_{yy}, \tilde{g} \ll \epsilon$ are the coupling constants, ϵ is the level splitting of the first (reference) qubit, and $|\delta| \ll \epsilon$ is the detuning. Here, the dots ... may represent additional terms (such as, e.g., XZ, ZX, etc.) that vanish in the rotating wave approximation. For realistic systems, $\epsilon \approx 10$ GHz, $g_{xx}, g_{yy} \approx 10$ MHz. For capacitive coupling, $g_{xx}, \tilde{g}=0$; for inductive coupling, $g_{yy}=0$, $\tilde{g} \lesssim 0.1 g_{xx}$.

In the doubly rotating frame (frame 1) defined by $e^{iH_0 t}(\ldots)e^{-iH_0 t}$, with $iH_0 \equiv -\epsilon(Z_1+Z_2)$, after averaging over fast oscillations and redefining the coupling constants, the system Hamiltonian is time independent,

$$iH_{\mathrm{RWA}} = -\delta Z_2 + i\mathcal{H} + \tilde{g}ZZ, \tag{12}$$

with

$$i\mathcal{H} = g(XX+YY) = ig\begin{pmatrix} 0 & 0 & 0 & 0 \\ 0 & 0 & 1 & 0 \\ 0 & 1 & 0 & 0 \\ 0 & 0 & 0 & 0 \end{pmatrix}. \tag{13}$$

Alternatively, to perform a useful consistency check, we consider another rotating frame (frame 2) defined by $e^{i\hat{H}_0 t}(\ldots)e^{-i\hat{H}_0 t}$, with $i\hat{H}_0 = -\epsilon(Z_1+Z_2) - \delta Z_2$. In this frame, the RWA Hamiltonian is

$$i\hat{H}_{\mathrm{RWA}}(t) = i\hat{\mathcal{H}}(t) + \tilde{g}ZZ, \tag{14}$$

where now we have a slowly varying interaction term given by

$$i\hat{\mathcal{H}}(t) = g[(XX+YY)\cos(\delta t) + (YX-XY)\sin(\delta t)] = ig\begin{pmatrix} 0 & 0 & 0 & 0 \\ 0 & 0 & e^{-i\delta t} & 0 \\ 0 & e^{+i\delta t} & 0 & 0 \\ 0 & 0 & 0 & 0 \end{pmatrix}. \tag{15}$$

The central block of this matrix has the form of a rotating drive for a spin-1/2 system whose analytical solution is well known [16]. This observation will prove helpful for calculations in Sec. III B. We will now show how these two RWA Hamiltonians lead to locally equivalent CNOT implementations.

B. Two-step control sequence

The well-known two-step CNOT control sequence for *resonant* ($\delta=0$) qubits is given by [15,17]

$$\mathrm{CNOT}_{(2)} = e^{i(\pi/4)}R_{\mathrm{post}}[U(t_{(2)}/2)e^{-\pi X_1}U(t_{(2)}/2)]R_{\mathrm{pre}}, \tag{16}$$

where

$$U(t_{(2)}/2) = e^{-(t_{(2)}/2)[g(XX+YY)+\tilde{g}ZZ]} = e^{-(t_{(2)}/2)\tilde{g}ZZ}\underbrace{\begin{pmatrix} 1 & 0 & 0 & 0 \\ 0 & 1/\sqrt{2} & -i/\sqrt{2} & 0 \\ 0 & -i/\sqrt{2} & 1/\sqrt{2} & 0 \\ 0 & 0 & 0 & 1 \end{pmatrix}}_{\equiv\sqrt{i\mathrm{SWAP}}}, \tag{17}$$

with

$$t_{(2)} = \pi/2g, \tag{18}$$

and $R_{\mathrm{post,pre}}$ are some local rotations. For future convenience we will choose

$$R_{\mathrm{post}} = e^{-(\pi/2)Y_2}, \quad R_{\mathrm{pre}} = e^{-(\pi/2)Z_2}e^{+(\pi/2)(X_2+X_1)}. \tag{19}$$

Of particular importance to us is the entangling part $U(t)e^{-\pi X_1}U(t)$ that determines the local equivalence class of the full gate. In our case the local class is controlled-NOT. We ask the following question:

If $|\delta| > 0$ (*detuned* qubits), can we still use Eq. (16) to generate the CNOT gate, possibly with *different* gate time and different pre- and postrotations? The answer to this question turns out to be "yes," provided δ is restricted in a certain way.

The time evolution operator is readily found to be

$$U(t) = e^{-t\tilde{g}ZZ}\begin{pmatrix} e^{i\delta t/2} & 0 & 0 & 0 \\ 0 & u & -iv & 0 \\ 0 & -iv & u^* & 0 \\ 0 & 0 & 0 & e^{-i\delta t/2} \end{pmatrix} \tag{20}$$

in frame 1, and

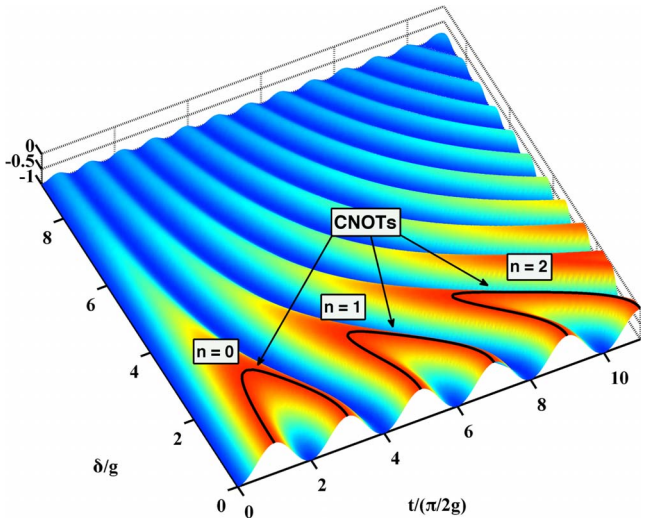

FIG. 1. (Color online) Makhlin invariants $-G_1(\delta,t)=-[G_2(\delta,t)-1]/2$ as functions of qubit detuning δ and the gate time t for the two-step control sequence of Sec. III. CNOT class corresponds to $G_1(\delta,t)=0$, $G_2(\delta,t)=1$. Notice that in order to implement perfect controlled-NOT logic, qubit detuning must be restricted to $|\delta|\leq 2g$, in accordance with Eqs. (24) and (26).

$$\hat{U}(t)=e^{-t\tilde{g}ZZ}\begin{pmatrix}1 & 0 & 0 & 0\\ 0 & ue^{-i\delta t/2} & -ive^{-i\delta t/2} & 0\\ 0 & -ive^{i\delta t/2} & u^{*}e^{i\delta t/2} & 0\\ 0 & 0 & 0 & 1\end{pmatrix} \tag{21}$$

in frame 2, where

$$u=\cos\left(\frac{\sqrt{\delta^2+4g^2}}{2}t\right)+\frac{i\delta}{\sqrt{\delta^2+4g^2}}\sin\left(\frac{\sqrt{\delta^2+4g^2}}{2}t\right),$$

$$v=\frac{2g}{\sqrt{\delta^2+4g^2}}\sin\left(\frac{\sqrt{\delta^2+4g^2}}{2}t\right). \tag{22}$$

In both frames the Makhlin invariants [14] of $U(t/2)e^{-\pi X_1}U(t/2)$ are independent of the ZZ coupling and are related to each other by

$$G_1=(G_2-1)/2$$
$$=\{\delta^2+8g^2\cos^2[(t/4)\sqrt{\delta^2+4g^2}]-4g^2\}^2/(\delta^2+4g^2)^2, \tag{23}$$

as shown in Fig. 1. Thus, for any t, the resulting gates are represented by the same point on the XX axis of the Weyl chamber (see [15,18] for discussion). Since CNOT class corresponds to $G_1=0$, $G_2=1$, we get

$$t_{(2)}^{\mp}=2\left(\frac{\pi(1+2n)\mp\arccos(\delta^2/4g^2)}{\sqrt{\delta^2+4g^2}}\right),\quad n=0,1,2,3,\ldots, \tag{24}$$

where n labels various branches of $t_{(2)}$ vs δ, and $\mp$ takes care of the double valuedness of each branch (see Fig. 1). The standard limit $t_{(2)}^{-}\to\pi/2g$ at $n=0$ is trivially recovered for vanishing detuning. In general, to fourth order in $\delta\to 0$,

$$t_{(2)}^{-}=(1+4n)[1/2g-\delta^2/16g^3+3\delta^4/256g^5]\pi$$
$$+\delta^2/4g^3-\delta^4/32g^5,$$

$$t_{(2)}^{+}=(3+4n)[1/2g-\delta^2/16g^3+3\delta^4/256g^5]\pi$$
$$-\delta^2/4g^3+\delta^4/32g^5. \tag{25}$$

Notice that the two-step control sequence works perfectly only when

$$|\delta|\leq 2g\ll\epsilon, \tag{26}$$

TABLE I. Two-step implementation of controlled-NOT logic using capacitively coupled Josephson phase qubits at finite detuning. Ideal CNOT generation is possible if detuning is restricted to $|\delta|\leq 2g$. At $|\delta|>2g$, the parameters are shown for gates closest to ideal CNOT in the sense of Eq. (2). Only minimal-time CNOTs are listed.

$\lvert\delta\rvert/g$	$t_{(2)}/(\pi/2g)$	G_1	G_2	c_1	c_2	$\mathcal{F}$
0.00	1.0000	0.0000	1.0000	1.0000	0.0000	1.0000
0.10	1.0003	0.0000	1.0000	1.0000	0.0000	1.0000
0.20	1.0014	0.0000	1.0000	1.0000	0.0000	1.0000
0.30	1.0031	0.0000	1.0000	1.0000	0.0000	1.0000
0.40	1.0056	0.0000	1.0000	1.0000	0.0000	1.0000
0.50	1.0088	0.0000	1.0000	1.0000	0.0000	1.0000
0.60	1.0128	0.0000	1.0000	1.0000	0.0000	1.0000
0.70	1.0177	0.0000	1.0000	1.0000	0.0000	1.0000
0.80	1.0235	0.0000	1.0000	1.0000	0.0000	1.0000
0.90	1.0303	0.0000	1.0000	1.0000	0.0000	1.0000
1.00	1.0383	0.0000	1.0000	1.0000	0.0000	1.0000
1.10	1.0476	0.0000	1.0000	1.0000	0.0000	1.0000
1.20	1.0585	0.0000	1.0000	1.0000	0.0000	1.0000
1.30	1.0713	0.0000	1.0000	1.0000	0.0000	1.0000
1.40	1.0863	0.0000	1.0000	1.0000	0.0000	1.0000
1.50	1.1043	0.0000	1.0000	1.0000	0.0000	1.0000
1.60	1.1261	0.0000	1.0000	1.0000	0.0000	1.0000
1.70	1.1536	0.0000	1.0000	1.0000	0.0000	1.0000
1.80	1.1901	0.0000	1.0000	1.0000	0.0000	1.0000
1.90	1.2445	0.0000	1.0000	1.0000	0.0000	1.0000
2.00	1.4142	0.0000	1.0000	1.0000	0.0000	1.0000
2.10	1.3793	0.0024	1.0048	0.9690	0.0000	0.9976
2.20	1.3453	0.0090	1.0181	0.9394	0.0000	0.9909
2.30	1.3124	0.0193	1.0386	0.9113	0.0000	0.9806
2.40	1.2804	0.0325	1.0650	0.8846	0.0000	0.9671
2.50	1.2494	0.0482	1.0964	0.8591	0.0000	0.9511
2.60	1.2194	0.0658	1.1316	0.8349	0.0000	0.9328
2.70	1.1905	0.0849	1.1698	0.8118	0.0000	0.9127
2.80	1.1625	0.1052	1.2104	0.7897	0.0000	0.8912
2.90	1.1355	0.1263	1.2526	0.7687	0.0000	0.8684
3.00	1.1094	0.1479	1.2959	0.7487	0.0000	0.8446

as illustrated in Fig. 1. When detuning exceeds this bound, the parameters for the gate closest to CNOT can be found in closed analytical form:

$$t_{(2)} = 2\pi(1+2n)/\sqrt{\delta^2+4g^2},$$

$$\vec{c} = [(2/\pi)\arccos(\sqrt{G_1}),0,0],$$

$$\mathcal{F} = -7 + 8\cos[(\pi/4)(c_1-1)]. \quad (27)$$

For $n=0$, these are shown in Table I.

We note in passing that the local pre- and postrotations [cf. Eq. (19)] generalize to

$$R_{\text{post}} = e^{-(\pi/2)Y_2} e^{-(\pi/2)(\alpha_2 Z_2 + \alpha_1 Z_1)},$$

$$R_{\text{pre}} = e^{-(\pi/2)[(1+\alpha_2)Z_2+\alpha_1 Z_1]} e^{+(\pi/2)(X_2+X_1)}, \quad (28)$$

in frame 1, where in the experimentally important case of minimal-time CNOT with $n=0$, to fourth order in $\delta \to 0$

$$\alpha_1^- = [8\pi(\delta/g) + (4-\pi)(\delta/g)^3]/(32\pi),$$

$$\alpha_2^- = [24(4+\pi)(\delta/g) + (16-3\pi)(\delta/g)^3]/(96\pi). \quad (29)$$

Also,

$$R_{\text{post}} = e^{-(\pi/2)Y_2} e^{-(\pi/2)\tilde{\beta}Z_2}, \quad R_{\text{pre}} = e^{-(\pi/2)(1+\beta)Z_2} e^{+(\pi/2)(X_2+X_1)}, \quad (30)$$

in frame 2.

To give an example, for capacitively coupled qubits at $\delta=1.00g$, the gate time is $t_{(2)}=1.0383(\pi/2g)$. The corresponding CNOT is given by Eq. (16), where now

$$U(t_{(2)}/2) = \begin{pmatrix} 0.9180+0.3965i & 0 & 0 & 0 \\ 0 & 0.6124+0.3536i & -0.7071i & 0 \\ 0 & -0.7071i & 0.6124-0.3536i & 0 \\ 0 & 0 & 0 & 0.9180-0.3965i \end{pmatrix}, \quad (31)$$

and $\alpha_2=0.5929$, $\alpha_1=0.2596$, in frame 1, and

$$\hat{U}(t_{(2)}/2) = \begin{pmatrix} 1 & 0 & 0 & 0 \\ 0 & 0.7024+0.0817i & -0.2804-0.6491i & 0 \\ 0 & 0.2804-0.6491i & 0.7024-0.0817i & 0 \\ 0 & 0 & 0 & 1 \end{pmatrix}, \quad (32)$$

and $\tilde{\beta}=-0.1858$, $\beta=0.3333$, in frame 2. Here, the local pre- and postangles required to generate the perfect CNOT gate have been found numerically.

On the other hand, at maximally allowed detuning $\delta=2.00g$, we have $t_{(2)}=1.4142(\pi/2g)$, and

$$U(t_{(2)}/2) = \begin{pmatrix} 0.4440+0.8960i & 0 & 0 & 0 \\ 0 & 0.7071i & -0.7071i & 0 \\ 0 & -0.7071i & -0.7071i & 0 \\ 0 & 0 & 0 & 0.4440-0.8960i \end{pmatrix}, \quad (33)$$

$\alpha_2=1.7071$, $\alpha_1=0.7071$, in frame 1, and

$$\hat{U}(t_{(2)}/2) = \begin{pmatrix} 1 & 0 & 0 & 0 \\ 0 & 0.6336+0.3140i & -0.6336-0.3140i & 0 \\ 0 & 0.6336-0.3140i & 0.6336-0.3140i & 0 \\ 0 & 0 & 0 & 1 \end{pmatrix}, \quad (34)$$

$\tilde{\beta}=-0.4142$, $\beta=1.0000$, in frame 2. The corresponding steering trajectory generating the CNOT gate in this case is shown in Fig. 2.

IV. SINGLE-STEP CNOT

In what follows, we will limit our discussion to Hamiltonians with $\tilde{g}=0$ (capacitive coupling only). In that case a single Rabi pulse suffices to implement single-step controlled-NOT logic [18]. When $\tilde{g}\neq 0$, local drives (one of

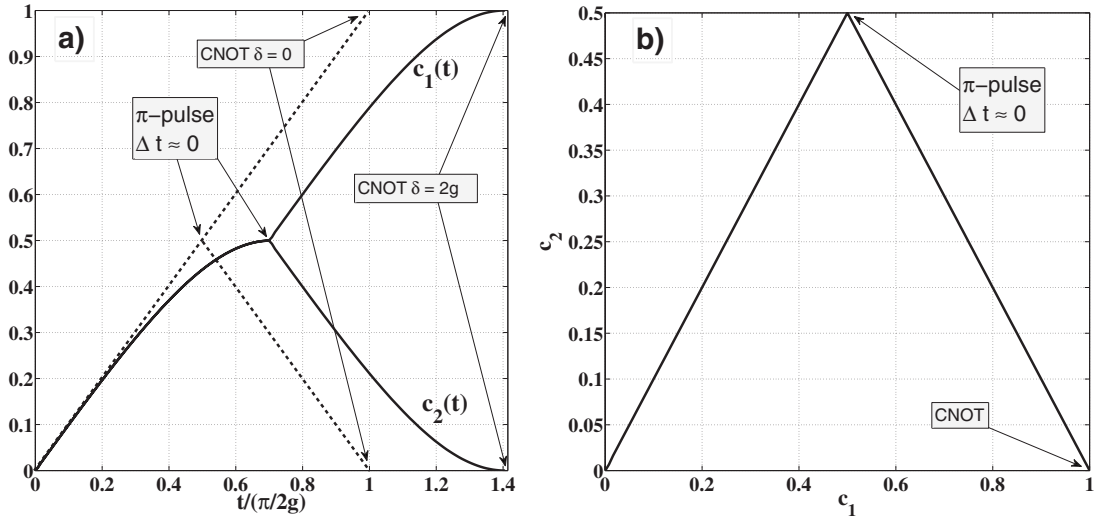

FIG. 2. Two-step CNOT implementation of entangling duration $t_{(2)}=\sqrt{2}(\pi/2g)$ for capacitively coupled Josephson phase qubits at maximally allowed detuning, $\delta=2g$. Panel (a): time dependence of the steering parameters $c_1(t)$ and $c_2(t)$. In the middle of the sequence, a fast π pulse is applied to one of the qubits. Dashed curves represent the resonant case, $\delta=0$. Panel (b): the corresponding steering trajectory on the Weyl chamber. Here, $c_3=0$ at all times.

which is much stronger than the other) must be applied to both qubits.

A. Resonant case

The Hamiltonian for two capacitively coupled resonant Josephson phase qubits, one of which is driven by a resonant rf pulse, is given by

$$iH(t) = -\epsilon(Z_1 + Z_2) + 2\Omega\cos(\epsilon t)X_1 + 2gYY, \tag{35}$$

where Ω is the corresponding Rabi frequency. Here we assume that $g \sim \Omega$, which differs from the condition $g \ll \Omega \ll \epsilon$ adopted in Ref. [9]. The RWA Hamiltonian (in frame 1) is then

$$iH_{\mathrm{RWA}} = \Omega X_1 + g(XX + YY), \tag{36}$$

with the corresponding CNOT sequence being [18]

$$\mathrm{CNOT}_{(1)} = e^{i(5\pi/4)}R_{\mathrm{post}}U(t_{(1)})R_{\mathrm{pre}}, \tag{37}$$

where

$$U(t_{(1)}) = e^{-t_{(1)}[\Omega X_1 + g(XX+YY)]} = \frac{(-1)^n}{\sqrt{2}}\begin{pmatrix} 1 & 0 & 0 & -i \\ 0 & 1 & -i & 0 \\ 0 & -i & 1 & 0 \\ -i & 0 & 0 & 1 \end{pmatrix}, \tag{38}$$

with

$$t_{(1)} = \pi/2g, \quad \Omega = g\sqrt{(4n)^2 - 1}, \quad n = 1,2,3,\ldots, \tag{39}$$

and

$$R_{\mathrm{post}} = e^{-(\pi/2)Y_2}, \quad R_{\mathrm{pre}} = e^{-(\pi/2)Z_2}e^{+(\pi/2)(X_2 - X_1)}. \tag{40}$$

Provided the RWA is still applicable, there is an infinite number of possible local drives, $\Omega/g = \sqrt{15} \approx 3.8730$, $\sqrt{63} \approx 7.9372$, and $\sqrt{143} \approx 11.9583$, that generate perfect CNOT gates of the same minimal duration $t_{(1)}/(\pi/2g) = 1$.

The corresponding graphs of $-d^{1/4}(\Omega, t)$ at $\delta = 0$ are shown in Figs. 3(a) and 6(a). (The extra minus sign and the exponent 1/4 are chosen to make the peaks representing CNOTs more pronounced.)

B. Nonresonant case

In the following sections we will generalize Eq. (37) to finite detuning, $\delta \neq 0$. Two physically distinct generalizations will be considered here depending on which of the two qubits is undergoing a local Rabi drive. Section IV B 1 deals with the case in which a resonant drive is applied to the reference qubit no. 1. Section IV B 2 considers the case in which a nonresonant drive is applied to the detuned qubit no. 2.

1. Driving the reference qubit

Here the Hamiltonian is given by

$$iH(t) = -\epsilon(Z_1 + Z_2) - \delta Z_2 + \underbrace{2\Omega\cos(\epsilon t)X_1}_{\text{reference qubit drive}} + 2gYY, \tag{41}$$

or,

$$iH_{\mathrm{RWA}} = -\delta Z_2 + \Omega X_1 + g(XX + YY). \tag{42}$$

The Makhlin invariants of the entangling part $U(t) = \exp(-iH_{\mathrm{RWA}}t)$ can be found in closed form, and are

$$G_1 = (1/4)(N_1 + N_2 + N_3 + N_4 + N_5)^2/(ABK)^4,$$

$$G_2 = (M_1 + M_2 + M_3 + M_4 + M_5 + M_6 + M_7)/(ABK^2)^2, \tag{43}$$

where

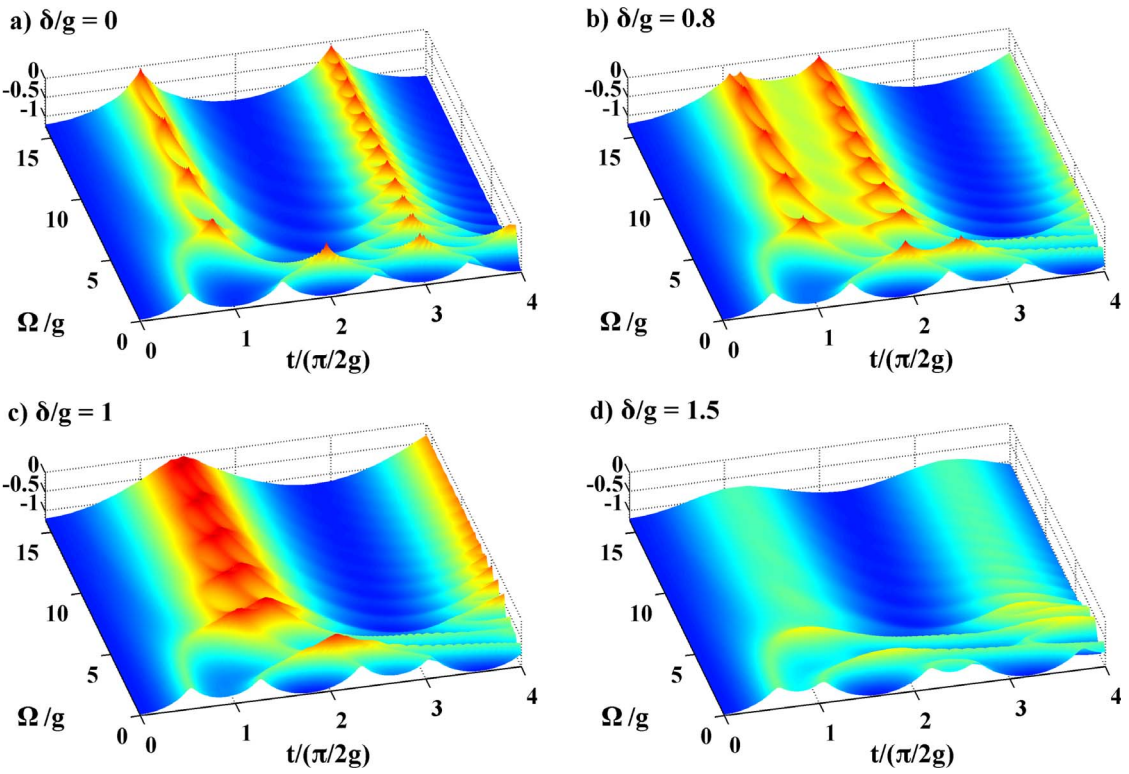

FIG. 3. (Color online) Graph of $[-d^{1/4}(\Omega,t)]$ as a function of entangling time t and Rabi frequency Ω at different values of detuning δ for the single-step implementation of Sec. IV B 1 in which a resonant local drive ΩX_1 is applied to the reference qubit no. 1. Singularities at $(-d^{1/4})=0$ correspond to various CNOT gates. Panels (a)–(c): as $|\delta|/g \to 1^-$, the two sets of CNOTs having $1<t/(\pi/2g)<3$ gradually approach each other while maintaining separation even at $|\delta|=g$. Panel (d): at larger values of detuning the graph flattens out and the distance function tends to its maximal constant value $d_{\max}=\sqrt{5}$. In this regime ($|\delta|>g$) perfect CNOT generation is no longer possible.

$$K=\sqrt{\Omega^2(\delta^2+g^2)+g^4},$$

$$A=\sqrt{\Omega^2+\delta^2+2(g^2+K)},\quad B=\sqrt{\Omega^2+\delta^2+2(g^2-K)}, \tag{44}$$

and

$$N_1=2\delta^2\{\Omega^6-\Omega^4(2\delta^2+g^2)-\Omega^2[g^4-\delta^2(\delta^2+3g^2)]+g^4(2g^2+\delta^2)\},$$

$$N_2=g^2[\Omega^4(\delta^2+g^2)+\Omega^2\delta^2(\delta^2-g^2-2K)+2\delta^2g^2(g^2+K)]\cos(At),$$

$$N_3=g^2[\Omega^4(\delta^2+g^2)+\Omega^2\delta^2(\delta^2-g^2+2K)+2\delta^2g^2(g^2-K)]\cos(Bt),$$

$$N_4=2\Omega^2g^2A^2B^2\cos(At/2)\cos(Bt/2),$$

$$N_5=2\Omega^2g^2(\Omega^2-\delta^2)AB\sin(At/2)\sin(Bt/2),$$

$$M_1=\delta^2g^8(3\delta^2+4g^2)+\Omega^8[3\delta^4+2g^2(\delta^2+g^2)]-2\delta^2\Omega^6[3\delta^4+2g^2(2\delta^2+g^2)]+\Omega^4(3\delta^8+10\delta^6g^2-2\delta^4g^4+4\delta^2g^6+g^8)+2\delta^2\Omega^2g^4[3\delta^4+g^2(7\delta^2-g^2)],$$

$$M_2=2\delta^2g^2(\Omega^2g^2+g^4+\Omega^2\delta^2)[\Omega^4+2g^2(g^2+K)+\Omega^2(\delta^2-g^2-2K)]\cos(At),$$

$$M_3=2\delta^2g^2(\Omega^2g^2+g^4+\Omega^2\delta^2)[\Omega^4+2g^2(g^2-K)+\Omega^2(\delta^2-g^2+2K)]\cos(Bt),$$

$$M_4=4\Omega^2g^2(\Omega^2\delta^2+g^4)[\Omega^4-2\Omega^2\delta^2+\delta^2(\delta^2+4g^2)]\cos(At/2)\cos(Bt/2),$$

$$M_5=4\Omega^2g^2\{\Omega^4\delta^2-\Omega^2[\delta^4+g^2(2\delta^2+g^2)]-\delta^2g^4\}AB\sin(At/2)\sin(Bt/2),$$

$$M_6=\Omega^4g^4[\Omega^4+2\Omega^2g^2+2g^2(2\delta^2+g^2)+\delta^4]\cos(At)\cos(Bt),$$

$$M_7=\Omega^4g^4(\Omega^2+2g^2+\delta^2)AB\sin(At)\sin(Bt). \tag{45}$$

The corresponding distance function is plotted in Fig. 3. Numerical analysis then shows that CNOT logic can only be generated exactly if detuning is restricted by

$$|\delta|\leq g\ll\epsilon. \tag{46}$$

The pre- and postrotations generalize to

$$R_{\text{post}}=e^{-(\pi/2)Y_2}e^{-(\pi/2)(\alpha_2Z_2+\alpha_1Z_1)},$$

$$R_{\text{pre}}=e^{-(\pi/2)[(1+\alpha_2)Z_2+\alpha_1Z_1]}e^{+(\pi/2)[X_2-(1+\gamma_1)X_1]}. \tag{47}$$

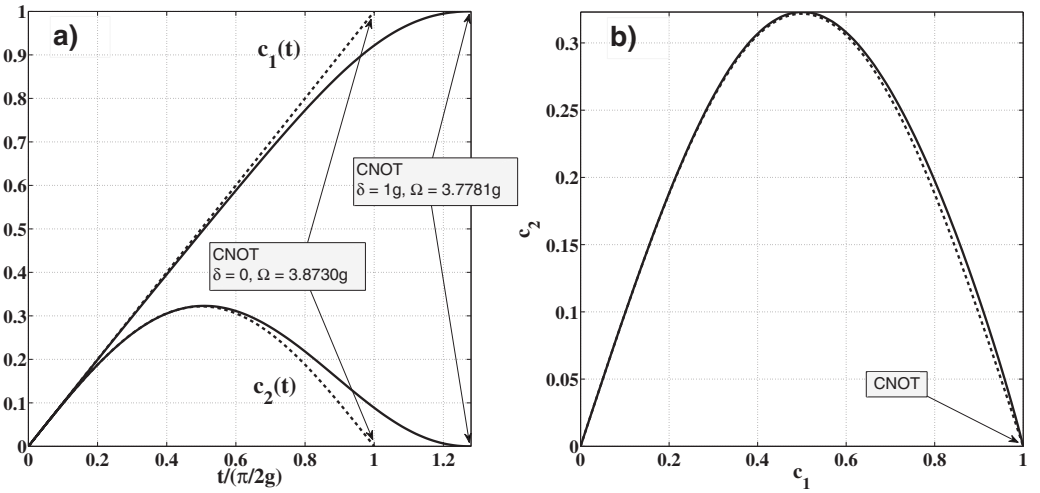

FIG. 4. Single-step CNOT implementation of entangling duration $t_{(1)}=1.2753(\pi/2g)$ and Rabi frequency $\Omega=3.7781g$ at maximally allowed detuning $\delta=g$ for implementation of Sec. IV B 1 in which the local drive ΩX_1 is applied to the reference qubit no. 1. Panel (a): time dependence of the steering parameters $c_1(t)$ and $c_2(t)$. Panel (b): the corresponding steering trajectory on the Weyl chamber. Here, $c_3=0$ at all times. Dashed curves represent the resonant case, $\delta=0$.

For example, at maximally allowed $\delta=1.00g$, we get $t_{(1)}=1.2753(\pi/2g)$ and $\Omega=3.7781g$. The resulting sequence is given in Eq. (37), where now the entangling part is

$$U(t_{(1)}) = e^{-t_{(1)}[-\delta Z_2+\Omega X_1+g(XX+YY)]} = \begin{pmatrix} -0.2552-0.4300i & 0.4823-0.1323i & -0.4823+0.1323i & 0.5i \\ 0.4823-0.1323i & -0.5i & 0.5i & 0.4823+0.1323i \\ -0.4823+0.1323i & 0.5i & 0.5i & 0.4823+0.1323i \\ 0.5i & 0.4823+0.1323i & 0.4823+0.1323i & -0.2552+0.4300i \end{pmatrix}, \tag{48}$$

and the local angles are $\alpha_2=0.8294$, $\alpha_1=-0.1705$, and $\gamma_1=-0.9998$. Figure 4 shows the Weyl chamber steering trajectory generating the CNOT class in this single-step example with $\delta=1.00g$.

For other values of qubit detuning, the gate parameters required to implement single-step CNOT logic are listed in Table II. Notice that when detuning exceeds the limits set in Eq. (46), our implementation begins to deviate from its perfect controlled-NOT form. Figure 5 shows the single-step steering trajectory simulated at $\delta=1.50g$ that has $t_{(1)}=1.0961(\pi/2g)$ and $\Omega=3.7152g$. Direct search for local pulses (not shown) results in the optimized gate,

$$U_{\text{opt}} = \begin{pmatrix} 0.9866 & -0.1122i & 0.0258i & 0.1158 \\ -0.1122i & 0.9866 & -0.1158 & -0.0258i \\ -0.1186 & 0.0009i & 0.1122i & 0.9866 \\ -0.0009i & 0.1186 & 0.9866 & 0.1122i \end{pmatrix}, \tag{49}$$

whose intrinsic fidelity with respect to the canonical CNOT gate is $\mathcal{F}=0.8927$.

To find the gate parameters in the experimentally important limit $\delta\to 0$, $t_{(1)}\to\pi/2g$, $\Omega\to\sqrt{15}g$, we write

$$t_{(1)} = \pi/2g + t_1(\delta/g) + t_2(\delta/g)^2 + \ldots,$$

$$\Omega = \sqrt{15}g + \Omega_1(\delta/g) + \Omega_2(\delta/g)^2 + \ldots. \tag{50}$$

Expanding $G_1=0$, $G_2=1$ to second order in δ and solving for t_1, t_2, Ω_1, Ω_2, gives

$$t_{(1)} = \pi/(2g)[1+(394-105\pi)(\delta/g)^2/(225\pi)],$$

$$\Omega = \sqrt{15}g[1+(3345\pi-10816)(\delta/g)^2/(6750\pi)]. \tag{51}$$

2. Driving the detuned qubit

In this case the Hamiltonian is given by

$$iH(t) = -\epsilon(Z_1+Z_2) - \delta Z_2 + \underbrace{2\Omega\cos(\epsilon t)X_2}_{\text{detuned qubit drive}} + 2gYY, \tag{52}$$

or,

$$iH_{\text{RWA}} = -\delta Z_2 + \Omega X_2 + g(XX+YY). \tag{53}$$

Here, the rf pulse is *not* resonant with the corresponding qubit. The Makhlin invariants of $U(t)=\exp(-iH_{\text{RWA}}t)$ are

$$G_1 = (N_1+N_2+N_3+N_4+N_5)^2/[A^2B^2(g^2+\Omega^2)]^2,$$

TABLE II. Single-step implementation of Sec. IV B 1 with the local drive ΩX_1 applied to the reference qubit no. 1. Ideal CNOT generation is possible if detuning is restricted to $|\delta| \leq g$. Only minimal-time CNOTs are listed.

$\lvert\delta\rvert/g$	$t_{(1)}/(\pi/2g)$	Ω/g	G_1	G_2	c_1	c_2	$\mathcal{F}$
0.00	1.0000	3.8730	0.0000	1.0000	1.0000	0.0000	1.0000
0.10	1.0009	3.8724	0.0000	1.0000	1.0000	0.0000	1.0000
0.20	1.0037	3.8707	0.0000	1.0000	1.0000	0.0000	1.0000
0.30	1.0085	3.8679	0.0000	1.0000	1.0000	0.0000	1.0000
0.40	1.0155	3.8638	0.0000	1.0000	1.0000	0.0000	1.0000
0.50	1.0253	3.8583	0.0000	1.0000	1.0000	0.0000	1.0000
0.60	1.0386	3.8513	0.0000	1.0000	1.0000	0.0000	1.0000
0.70	1.0568	3.8422	0.0000	1.0000	1.0000	0.0000	1.0000
0.80	1.0827	3.8303	0.0000	1.0000	1.0000	0.0000	1.0000
0.90	1.1245	3.8132	0.0000	1.0000	1.0000	0.0000	1.0000
1.00	1.2753	3.7781	0.0000	1.0000	1.0000	0.0000	1.0000
1.10	1.2330	3.7470	0.0030	0.9994	0.9653	0.0365	0.9937
1.20	1.1945	3.7323	0.0106	0.9978	0.9339	0.0695	0.9773
1.30	1.1590	3.7250	0.0214	0.9955	0.9054	0.0994	0.9536
1.40	1.1262	3.7203	0.0340	0.9927	0.8795	0.1267	0.9248
1.50	1.0961	3.7152	0.0476	0.9898	0.8559	0.1514	0.8927
1.60	1.0686	3.7074	0.0614	0.9867	0.8344	0.1740	0.8585
1.70	1.0438	3.6952	0.0749	0.9837	0.8147	0.1946	0.8232
1.80	1.0216	3.6772	0.0879	0.9808	0.7966	0.2134	0.7875
1.90	1.0019	3.6519	0.1003	0.9780	0.7801	0.2307	0.7519
2.00	0.9849	3.6179	0.1118	0.9754	0.7648	0.2466	0.7168

$$G_2 = (M_1 + M_2 + M_3 + M_4 + M_5 + M_6 + M_7)^2/[AB(g^2 + \Omega^2)]^2, \tag{54}$$

where

$$A = \sqrt{\delta^2 + 2g^2 + \Omega^2 + 2g\sqrt{g^2 + \Omega^2}},$$

$$B = \sqrt{\delta^2 + 2g^2 + \Omega^2 - 2g\sqrt{g^2 + \Omega^2}}, \tag{55}$$

and

$$N_1 = -g^2(\Omega^4 - \delta^4),$$

$$N_2 = \Omega^2(AB)^2 \cos(At/2)\cos(Bt/2),$$

$$N_3 = \Omega^2(\Omega^2 + \delta^2)AB \sin(At/2)\sin(Bt/2),$$

$$N_4 = g^2[\Omega^4 + \delta^2(A^2 - \delta^2)]\cos^2(At/2),$$

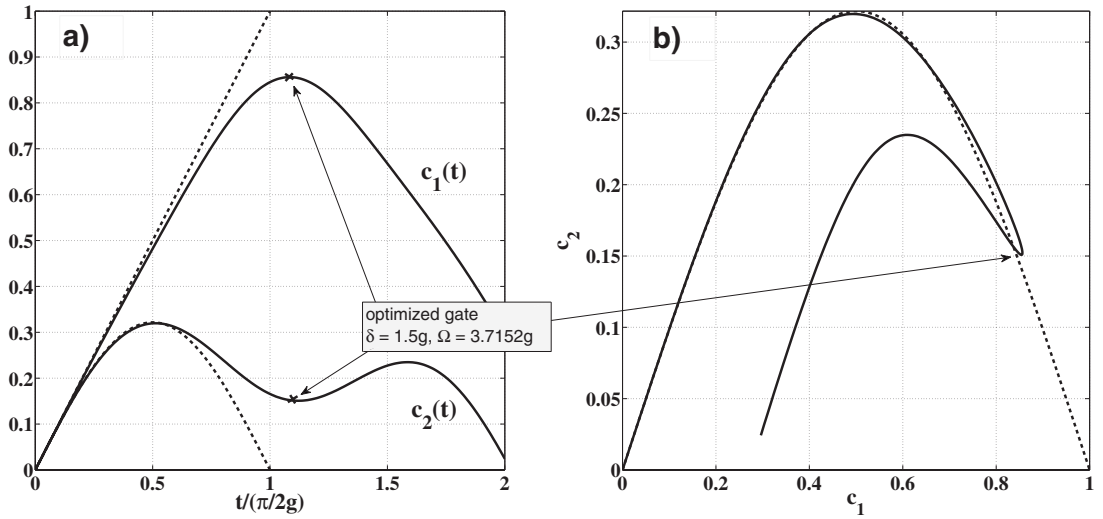

FIG. 5. Single-step implementation generating the gate closest to CNOT in terms of Eq. (2) at $\delta = 1.5g$ for implementation of Sec. IV B 1 in which the local drive ΩX_1 is applied to the reference qubit no. 1. Panel (a): time dependence of the steering parameters $c_1(t)$ and $c_2(t)$. Closest class is reached at $t_{(1)} = 1.0961(\pi/2g)$ and has $\Omega = 3.7152g$. Panel (b): the corresponding steering trajectory on the Weyl chamber. Here, $c_3 = 0$ at all times. Dashed curves represent the resonant case, $\delta = 0$.

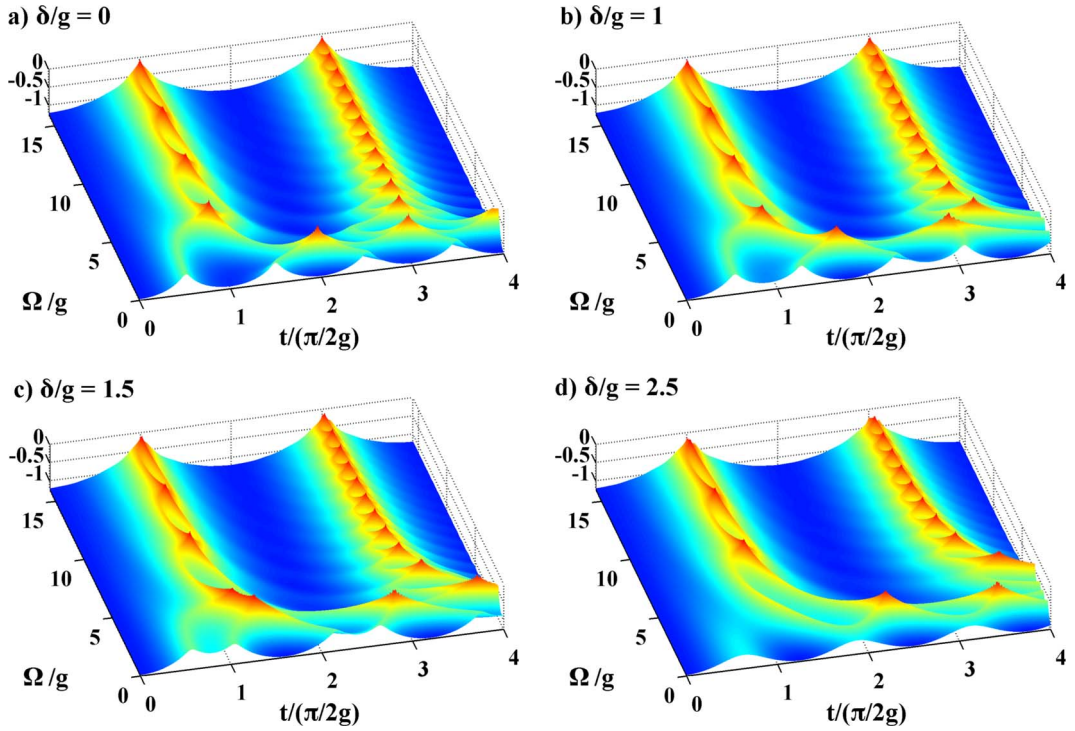

FIG. 6. (Color online) Graph of $[-d^{1/4}(\Omega,t)]$ as a function of entangling time t and Rabi frequency Ω at different values of detuning δ for the single-step implementation of Sec. IV B 2, in which a nonresonant local drive ΩX_2 is applied to the detuned qubit no. 2. The peaks at $(-d^{1/4})=0$ correspond to various controls that generate the CNOT equivalence class. Panels (a)–(c): notice how a pair of CNOTs having $\Omega/g<\sqrt{15}$ and $1<t/(\pi/2g)<2$ gradually disappears as detuning increases. (This process repeats itself for other pairs of CNOTs at larger detuning.) Panel (d): minimal-time CNOTs ($t\approx\pi/2g$) can be generated at any δ provided Ω is chosen to be sufficiently large.

$$N_5 = g^2[\Omega^4 + \delta^2(B^2 - \delta^2)]\cos^2(Bt/2),$$

$$M_1 = 2\Omega^8 + 4\Omega^6\delta^2 + \Omega^4(2\delta^4 + 8\delta^2g^2 + g^4) + 2\Omega^2\delta^2g^2(\delta^2 + g^2) + 3\delta^4g^4 + 4\delta^2g^6,$$

$$M_2 = 2\delta^2g^2[\Omega^4 + g\Omega^2(3g + 2\sqrt{g^2+\Omega^2}) + 2g^3(g + \sqrt{g^2+\Omega^2})]\cos(At),$$

$$M_3 = 2\delta^2g^2[\Omega^4 + g\Omega^2(3g - 2\sqrt{g^2+\Omega^2}) + 2g^3(g - \sqrt{g^2+\Omega^2})\cos(Bt),$$

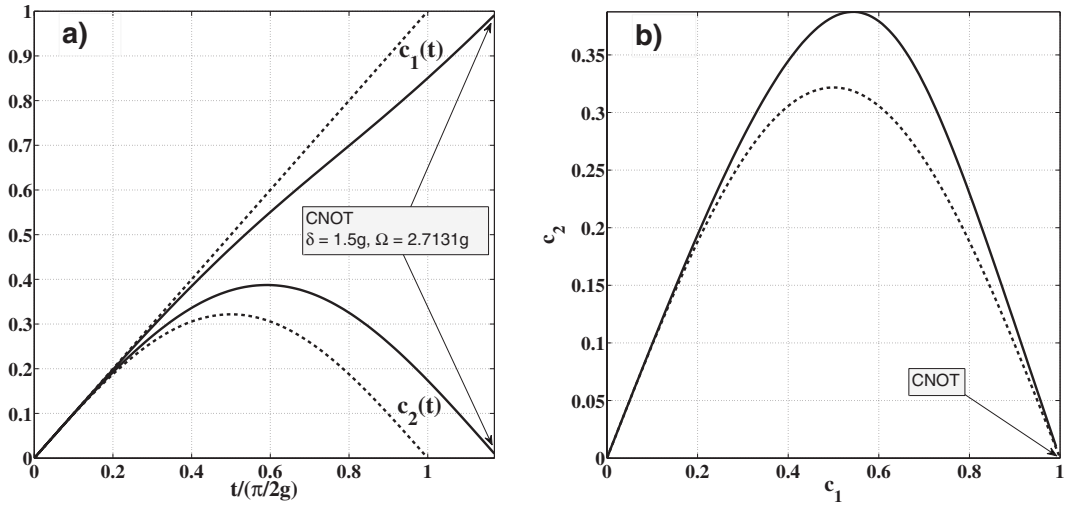

FIG. 7. Single-step CNOT implementation with $t_{(1)}=1.1794(\pi/2g)$, $\Omega=2.7131g$, at subcritical detuning $\delta=1.5g$ for implementation of Sec. IV B 2 in which the local drive ΩX_2 is applied to the detuned qubit no. 2. Panel (a): time dependence of the steering parameters $c_1(t)$ and $c_2(t)$. Panel (b): the corresponding steering trajectory on the Weyl chamber. Here, $c_3=0$ at all times. Dashed curves represent the resonant case, $\delta=0$.

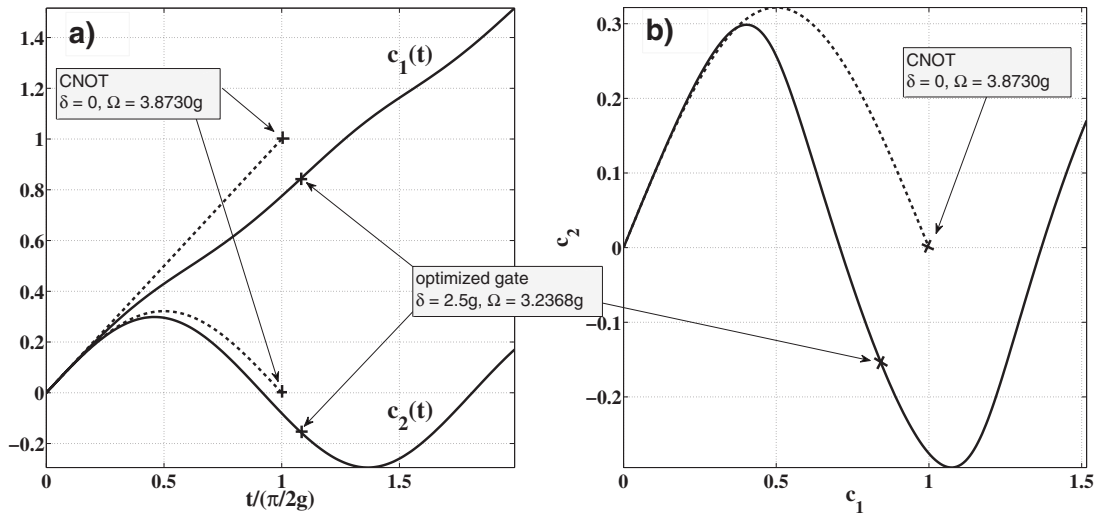

FIG. 8. Single-step implementation generating the gate closest to CNOT in the sense of Eq. (2) at $\delta=2.5g$ for implementation of Sec. IV B 2 in which the local drive ΩX_2 is applied to the detuned qubit no. 2. Panel (a): time dependence of the steering parameters $c_1(t)$ and $c_2(t)$. The gate has $t_{(1)}=1.0865(\pi/2g)$ and $\Omega=3.2368g$. Panel (b): the corresponding steering trajectory on the Weyl chamber. Here, $c_3=0$ at all times. Dashed curves represent the resonant case, $\delta=0$.

TABLE III. Single-step implementation of Sec. IV B 2 with the local drive ΩX_2 applied to the detuned qubit no. 2.

$\lvert\delta\rvert/g$	$t_{(1)}/(\pi/2g)$	Ω/g	G_1	G_2	c_1	c_2	$\mathcal{F}$
0.00	1.0000	3.8730	0.0000	1.0000	1.0000	0.0000	1.0000
0.10	1.0004	3.8698	0.0000	1.0000	1.0000	0.0000	1.0000
0.20	1.0016	3.8600	0.0000	1.0000	1.0000	0.0000	1.0000
0.30	1.0036	3.8437	0.0000	1.0000	1.0000	0.0000	1.0000
0.40	1.0064	3.8205	0.0000	1.0000	1.0000	0.0000	1.0000
0.50	1.0102	3.7902	0.0000	1.0000	1.0000	0.0000	1.0000
0.60	1.0149	3.7523	0.0000	1.0000	1.0000	0.0000	1.0000
0.70	1.0208	3.7061	0.0000	1.0000	1.0000	0.0000	1.0000
0.80	1.0280	3.6509	0.0000	1.0000	1.0000	0.0000	1.0000
0.90	1.0368	3.5853	0.0000	1.0000	1.0000	0.0000	1.0000
1.00	1.0474	3.5077	0.0000	1.0000	1.0000	0.0000	1.0000
1.10	1.0605	3.4155	0.0000	1.0000	1.0000	0.0000	1.0000
1.20	1.0768	3.3047	0.0000	1.0000	1.0000	0.0000	1.0000
1.30	1.0982	3.1678	0.0000	1.0000	1.0000	0.0000	1.0000
1.40	1.1281	2.9888	0.0000	1.0000	1.0000	0.0000	1.0000
1.50	1.1794	2.7131	0.0000	1.0000	1.0000	0.0000	1.0000
1.54	1.2259	2.4928	0.0000	1.0000	1.0000	0.0000	1.0000
1.60	1.2536	2.3693	0.0003	0.9999	0.9891	0.0115	0.9994
1.70	1.2332	2.4501	0.0024	0.9995	0.9688	0.0328	0.9949
1.80	1.2132	2.5343	0.0062	0.9986	0.9498	0.0529	0.9869
1.90	1.1936	2.6220	0.0112	0.9975	0.9321	0.0716	0.9760
2.00	1.1745	2.7132	0.0172	0.9961	0.9155	0.0891	0.9628
2.10	1.1559	2.8083	0.0238	0.9945	0.9000	0.1055	0.9480
2.20	1.1378	2.9074	0.0308	0.9929	0.8856	0.1207	0.9319
2.30	1.1203	3.0112	0.0380	0.9911	0.8722	0.1349	0.9151
2.40	1.1032	3.1206	0.0451	0.9892	0.8599	0.1480	0.8980
2.50	1.0865	3.2368	0.0521	0.9873	0.8485	0.1601	0.8808

$$M_4 = \Omega^4[\Omega^4 + 2\Omega^2(\delta^2 + g^2) + (\delta^4 + 4\delta^2 g^2 + 2g^4)]\cos(At)\cos(Bt),$$

$$M_5 = \Omega^4[\Omega^2 + (\delta^2 + 2g^2)]AB\,\sin(At)\sin(Bt),$$

$$M_6 = 4\Omega^2 g^2[\Omega^4 + 2\Omega^2\delta^2 + \delta^2(\delta^2 + 4g^2)]\cos(At/2)\cos(Bt/2),$$

$$M_7 = -4\Omega^2 g^2(\Omega^2 - \delta^2)AB\,\sin(At/2)\sin(Bt/2). \quad (56)$$

In the limit $\delta \to 0$, $t_{(1)} \to \pi/2g$, $\Omega \to \sqrt{15}g$, to the second order in δ,

$$t_{(1)} = (\pi/2g)[1 + (15\pi + 8)(\delta/g)^2/(450\pi)],$$

$$\Omega = \sqrt{15}g[1 - 16(15\pi + 8)(\delta/g)^2/(3375\pi)]. \quad (57)$$

The corresponding distance function is plotted in Fig. 6. In this case, the pre- and postrotations have the form

$$R_{\text{post}} = e^{-(\pi/2)(1+\gamma_2)Y_2} e^{-(\pi/2)\alpha(Z_2+Z_1)},$$

$$R_{\text{pre}} = e^{-(\pi/2)[(1+\alpha)Z_2+\alpha Z_1]} e^{+(\pi/2)[(1+\gamma_2)X_2 - X_1]}. \quad (58)$$

Figure 7 shows the trajectory generated at subcritical value of detuning $\delta = 1.50g$. The exact CNOT is reached at $t_{(1)} = 1.1794(\pi/2g)$, provided the Rabi frequency is set to $\Omega = 2.7131g$, and the local angles are chosen to be $\alpha = -0.1156$, $\gamma_2 = -0.3260$. In this case,

$$U(t_{(1)}) = e^{-t_{(1)}[-\delta Z_2 + \Omega X_2 + g(XX+YY)]} = \begin{pmatrix} -0.6610 + 0.2512i & -0.0626 - 0.3408i & 0 & 0.6164i \\ -0.0626 - 0.3408i & -0.7071 & 0.6164i & 0 \\ 0 & 0.6164i & -0.7071 & -0.0626 + 0.3408i \\ 0.6164i & 0 & -0.0626 + 0.3408i & -0.6610 - 0.2512i \end{pmatrix}. \quad (59)$$

Figure 8 shows how the gate closest to CNOT is reached at $\delta = 2.50g$, which is greater than the maximally allowed detuning ($\delta \approx 1.54g$) for this range of Rabi frequencies ($\Omega \approx \sqrt{15}g$). For other values of local controls, see Table III.

The most important feature of this implementation is that it allows generation of exact CNOT logic at *any* value of qubit detuning, as long as the amplitude of nonresonant pulse can be chosen to be sufficiently large. For instance, at the above-mentioned $\delta = 2.50g$ it is still possible to make a perfect CNOT gate of short duration $t_{(1)} = 1.0650(\pi/2g)$ by setting $\Omega = 6.9836g$ [as depicted in Fig. 6(d)].

V. CONCLUSION

In summary, we have demonstrated that various CNOT control sequences previously proposed for resonant Josephson phase qubits may still be used at finite detuning. To achieve high fidelity of the resulting gate the value of the detuning during the entangling operations should not be greater than $2g$ in the two-step implementation and g in the single-step implementation with the locally driven reference qubit. When a specially chosen local nonresonant drive is applied to the detuned qubit, perfect CNOT generation is possible at any δ provided that the pulse strength can be made arbitrarily large.

ACKNOWLEDGMENTS

This work was supported by IARPA under Grant No. W911NF-08-1-0336 and by the NSF under Grant No. CMS-0404031. The author thanks Michael Geller and John Martinis for useful discussions.

[1] Y. Yamamoto, Y. A. Pashkin, O. Astafiev, Y. Nakamura, and J. S. Tsai, Nature (London) **425**, 941 (2003).
[2] A. J. Berkley, H. Xu, R. C. Ramos, M. A. Gubrud, F. W. Strauch, P. R. Johnson, J. R. Anderson, A. J. Dragt, C. J. Lobb, and F. C. Wellstood, Science **300**, 1548 (2003).
[3] V. Corato, P. Silvestrini, L. Stodolsky, and J. Wosiek, Phys. Rev. B **68**, 224508 (2003).
[4] J. Q. You and F. Nori, Phys. Today **58** (11), 42 (2005).
[5] M. Steffen, M. Ansmann, R. C. Bialczak, N. Katz, E. Lucero, R. McDermott, M. Neeley, E. M. Weig, A. N. Cleland, and J. M. Martinis, Science **313**, 1423 (2006).
[6] J. H. Plantenberg, P. C. de Groot, C. J. Harmans, and J. E. Mooij, Nature (London) **447**, 836 (2007).
[7] M. J. Testolin, C. D. Hill, C. J. Wellard, and L. C. L. Hollenberg, Phys. Rev. A **76**, 012302 (2007).
[8] A. Galiautdinov and J. M. Martinis, Phys. Rev. A **78**, 010305(R) (2008).
[9] C. Rigetti, A. Blais, and M. Devoret, Phys. Rev. Lett. **94**, 240502 (2005).
[10] J. Li, K. Chalapat, and G. S. Paraoanu, Phys. Rev. B **78**, 064503 (2008).
[11] P. R. Johnson, F. W. Strauch, A. J. Dragt, R. C. Ramos, C. J.

Lobb, J. R. Anderson, and F. C. Wellstood, Phys. Rev. B **67**, 020509(R) (2003).

[12] B. L. T. Plourde, J. Zhang, K. B. Whaley, F. K. Wilhelm, T. L. Robertson, T. Hime, S. Linzen, P. A. Reichardt, C.-E. Wu, and John Clarke, Phys. Rev. B **70**, 140501(R) (2004).

[13] J. Majer, J. M. Chow, J. M. Gambetta, J. Koch, B. R. Johnson, J. A. Schreier, L. Frunzio, D. I. Schuster, A. A. Houck, A. Wallraff, A. Blais, M. H. Devoret, S. M. Girvin, and R. J. Schoelkopf, Nature (London) **449**, 443 (2007).

[14] Yu. Makhlin, Quantum Inf. Process. **1**, 243 (2002).

[15] J. Zhang, J. Vala, S. Sastry, and K. B. Whaley, Phys. Rev. A **67**, 042313 (2003).

[16] Recall that for a two-level system driven by the Hamiltonian $H=\epsilon_0\sigma^z/2+g[\sigma^x\cos(\delta t)+\sigma^y\sin(\delta t)]$, the corresponding time evolution operator is given by $U(t)=e^{-i\delta t(\sigma^z/2)}\times e^{-i[(\epsilon_0-\delta)(\sigma^z/2)+g\sigma^x]t}$. Equation (15) corresponds to $\epsilon_0=0$.

[17] G. Burkard, D. Loss, D. P. DiVincenzo, and J. A. Smolin, Phys. Rev. B **60**, 11404 (1999).

[18] A. Galiautdinov, Phys. Rev. A **75**, 052303 (2007); J. Math. Phys. **48**, 112105 (2007).